Detecting trends in bottom pressure measured using a tall mooring and altimetry

Joanne Williams,[1] Chris W. Hughes,[1,2] Mark E. Tamisiea,[1]

Corresponding author: Joanne Williams, National Oceanography Centre, Joseph Proudman

Building, 6 Brownlow St, Liverpool L3 5DA, UK. (joll@noc.ac.uk)

[1]National Oceanography Centre,

Liverpool, UK.

[2]School of Environmental Sciences,

University of Liverpool, Liverpool, UK.

Abstract.   Stable, accurate measurements of ocean bottom pressure would be valuable for a range of purposes, including ocean circulation monitoring and measurement of the mass component of the changing sea level budget. Geographic variability of bottom pressure is in general smaller than variability of sea level, particularly at equatorial sites. However existing bottom pressure recorder technology suffers from drift of several cm/yr, too much for practical realization of these purposes.

Therefore we investigate the use of a tall hydrographic mooring to detect trends in ocean bottom pressure, using data from the Rapid experiment in the North Atlantic. The accuracy of the method is dependent on the number of instruments on the mooring, and we demonstrate how an ocean model (in our case NEMO) can be used to provide an estimate of accuracy of this technique and hence guide mooring design. We also show how it is also dependent on the operational calibration of instruments. We find that, together with altimetry and sea-surface temperatures, such a mooring can be used to provide bottom pressure variations to within about 1 mbar (1 cm sea-level). We estimate that an optimally calibrated mooring in the North Atlantic could detect a trend in bottom pressure to an accuracy of ± 1 mm/year after approximately 12 years of operation.

1. Introduction

Ocean bottom pressure (BP) measurements are a useful tool in the study of global sea-level, and in distinguishing the sea-level rise due to increasing ocean mass from that due to reduction of density. We have previously shown [*Hughes et al.*, 2012; *Williams et al.*, 2014] that BP records from the deep equatorial ocean can be used to find the annual cycle of ocean mass, and could theoretically be used to find a trend in ocean mass. Those results implied that measuring BP at even a few locations in this region could constrain the trend of global-average ocean mass. However, this is impossible with existing bottom pressure recorder (BPR) technology, as instruments suffer from drift [*Watts and Kontoyiannis*, 1990].

Because of the strong dynamical constraints on BP variability [*Hughes and de Cuevas*, 2001], BP is also a powerful diagnostic of ocean circulation. So much so that, despite the instrumental limitations, BP measurements have played an important role in monitoring large-scale ocean phenomena such as the flow through Drake Passage [*Hughes et al.*, 1999; *Meredith et al.*, 2011; *Chereskin et al.*, 2012] and the North Atlantic meridional overturning circulation [*Rayner et al.*, 2011; *Hughes et al.*, 2013; *Elipot et al.*, 2013a, b]. They have also provided vital base information for several large experiments designed to monitor energetic mesoscale variability [*Watts et al.*, 2001; *Howe et al.*, 2009; *Chereskin et al.*, 2012].

Attempts have been made to characterize the BPR instrument drift, with the usual approach being to fit a linear-plus-exponential model [*Watts and Kontoyiannis*, 1990; *Polster et al.*, 2009]. The decaying exponential usually has a time scale of months, and

the linear part varies in both magnitude and sign between instruments and redeployments of the same instrument. We have seen records with drifts of up to 20 cm/yr [*Williams et al.*, 2014]. Without precise calibration or an understanding of the physical mechanism of the drift, even with multiple instruments on the same mooring one cannot isolate the linear drift from a true trend in BP.

Therefore this study examines the possibility of using other existing records to calculate the BP of the ocean. Can we use long-term hydrographic moorings, together with satellite altimetry, to measure BP? Before considering trend detection, we must first assess the accuracy of this technique in reproducing BP. We will use the data from the Rapid campaign at 26°N in the Atlantic, as the best available long-term records of tall CTD moorings and BPRs. We will investigate sources of error in this comparison, including non-linear drift on the BPRs and issues with the mooring instruments including the accuracy of calibration. We will assess the error due to the vertical sampling on the mooring, and demonstrate that the NEMO global ocean circulation model can be used to give a good estimate of the sampling error.

Note that the steric and sea-level signals largely cancel to produce the much smaller BP variability. Thus, the relevant question is not if individual observations of recorded and reconstructed BP are identical, but if the two signals agree to within the uncertainty estimated through the ocean model. If this is the case, then we can have confidence in using the model to assess the uncertainties in the trend calculations.

Our study complements global studies [e.g. *Chambers and Willis*, 2010] comparing satellite altimetry (sea level) and ARGO (density) with ocean bottom pressure inferred from GRACE (gravity), by showing how a single mooring can complement these methods.

Trend detection depends on the variability of the underlying signal [*Hughes and Williams*, 2010]. BP has advantages over sea level in this regard, and we will show that the time required to detect a trend to an accuracy of 1 mm/yr, even allowing for measurement errors, is less than for sea-level, and only a few years longer than the existing measurement campaigns. We focus attention on calculation of errors in the density component of the budget. Long-term trend errors in satellite altimetry are a complex issue which is currently receiving attention elsewhere [e.g. *Ablain et al.*, 2015].

2. Method

Let us first consider the relationship between BP and sea-level. Using hydrostatic balance, the total depth of the sea at a given location may be written

$$\eta + H = \int_{p_b}^{p_a} \frac{dz}{dp}\, dp = \int_{p_a}^{p_b} \frac{v(p,t)}{g(z)}\, dp,\tag{1}$$

where $v = 1/\rho$ is the specific volume, ρ is density, g is acceleration due to gravity, p_b is ocean bottom pressure, and p_a is atmospheric pressure. Here the sea-surface height (SSH) is at $z = \eta$ measured relative to any fixed reference level (such as the reference ellipsoid used in satellite altimeter measurements), and the position of the seafloor $z = -H$ is defined relative to the same reference (we imagine that reference to be close to the sea surface, so that H represents approximate ocean depth). Note that $z = 0$ is not a geoid or equipotential surface. Introducing constant pressures p_{a_0} and p_{b_0}, close to the atmospheric pressure and bottom pressure respectively, the pressure integral can be split into three ranges giving

$$\eta(t) + H(t) = \int_{p_{b_0}}^{p_{b(t)}} \frac{v(p,t)}{g(z)}\, dp + \int_{p_{a_0}}^{p_{b_0}} \frac{v(p,t)}{g(z)}\, dp + \int_{p_a(t)}^{p_{a_0}} \frac{v(p,t)}{g(z)}\, dp.\tag{2}$$

If we assume that $g = g_b$ and $v = 1/\rho_b$, independent of depth over the narrow pressure range $p_{b_0} < p < p_b(t)$, and $g = g_a$ and $v = 1/\rho_a$ in the range $p_a(t) < p < p_{a_0}$, then this simplifies and rearranges to give

$$\frac{p_b(t) - p_{b_0}}{\rho_b(t)g_b} = \eta(t) + H(t) - \int_{p_{a_0}}^{p_{b_0}} \frac{v(p,t)}{g(z)}\,dp + \frac{p_a(t) - p_{a_0}}{\rho_a(t)g_a}. \tag{3}$$

Here, the left hand side is small (typically cm), the first and last terms on the right hand side are similarly small and represent SSH and the inverse barometer correction to sea level, and the remaining two terms are large ($\approx$5000 m) and strongly canceling, representing the depth of the ocean relative to the reference surface (ellipsoid), and the thickness of the reference water column between surface and bottom reference pressures p_{a_0} and p_{b_0}.

Steric sea level is conventionally expressed in terms of a specific volume anomaly $v' = v - v_r(p)$ relative to a reference specific volume for water of a particular reference composition at the same pressure. If we write

$$p'_a(t) = p_a(t) - p_{a_0},$$

$$p'_b(t) = p_b(t) - p_{b_0},$$

$$\eta'(t) + H'(t) = \eta(t) + H(t) - \int_{p_{a_0}}^{p_{b_0}} \frac{v_r(p)}{g(p)}\,dp, \tag{4}$$

then we can rewrite (3) as

$$\frac{p'_b(t)}{\rho_b(t)g_b} = \eta'(t) + H'(t) - \int_{p_{a_0}}^{p_{b_0}} \frac{v'(p,t)}{g(p)}\,dp + \frac{p'_a(t)}{\rho_a(t)g_a}, \tag{5}$$

where all terms are now of the same order, with the pressure integral representing a more conventional steric sea level. (Strictly, ignoring the distinction between $g(z)$ and $g(p)$ introduces some time dependence in (4). However the z value for which a given p occurs is only varying by order 0.1 m, so the size of this error is $\approx 1.6 \times 10^{-8}g$. Integrating this

error over 5000 m introduces a pressure error of $\approx$ 0.8 Pa, or 0.08 mm, less than 0.1% of the signal variance. We therefore ignore this distinction.)

In (5), small vertical differences in values of g and changes with time of bottom density no longer multiply large terms and are of little concern. Thus we introduce constant values of these terms of $g = 9.8$ ms^{-2} and ρ_{b_0}. Then (5) can be approximated as

$$p'_b(t) \approx g\rho_{b_0}[\eta'(t) + H'(t)] - \rho_{b_0} \int_{p_{a_0}}^{p_{b_0}} v'(p,t)\, dp + p'_a(t)\frac{\rho_{b_0}}{\rho_a(t)}, \qquad (6)$$

showing how bottom pressure variations can be calculated from sea level variations, density variations at given pressure (as determined from hydrographic data), and atmospheric pressure variations. In principle, we also need to know the motion of the seafloor $H'(t)$, but we will neglect this in our calculations. This assumption will be discussed in more detail later. Aside from the seafloor term, the right-hand side in (6) represents the inverse barometer corrected sea level, and the steric sea level. In the deep open ocean where baroclinic variability dominates on timescales longer than a few months, the expectation is that dynamical bottom pressure changes represent a small residual of these larger signals [*Vinogradova et al.*, 2007; *Bingham and Hughes*, 2008].

Note that the bottom density rather than surface density multiplies the surface terms η' and p'_a/ρ_a. This is an effect of the compressibility of seawater [*Ray*, 2013; *Wahr et al.*, 2014].

2.1. Steric calculation
2.1.1. Source of mooring data

For the steric pressure we use temperature and salinity data from the Rapid mooring array near 26° N in the Atlantic [*Hirschi et al.*, 2003], and downloaded from the British

Oceanographic Data Centre (BODC). We select "tall" moorings, with instruments at depths from the ocean floor to within at most 200 m of the surface, for which there are several years of data, and where there exist co-located bottom pressure measurements for at least part of the record. Data was provided as instantaneous measurements at 10, 15, or 30 minute intervals (not necessarily on the hour) and interpolated onto hourly intervals.

On these criteria there are two moorings from the Western boundary array (WB2: 76.74° W, 26.51° N and WB5: 71.97° W, 26.49° N), one from the mid-Atlantic ridge (MAR1: 49.72° W, 24.18° N) and one from the Eastern boundary array (EB1: 24.10° W, 23.85° N); further details are given in Figure 1. The moorings have no surface buoys. The number and depth of instruments varies between deployments, with around 15–30 instruments, discounting failures and overlaps. Nominal instrument depths are listed in supplementary information tables S1–S4. The nominal pressure of the instruments on each mooring, and actual pressures recorded by the instruments, are shown later as part of figures 5–8. The maximum pressure recorded at the moorings are approximately 3975 dbar (WB2), 5296 dbar (WB5), 5327 dbar (MAR1) and 5202 dbar (EB1).

2.1.2. Source of sea-surface temperature data (SST)

Since the moorings do not include instruments at the surface, additional data on temperature at the sea surface were taken from the Advanced Microwave Scanning Radiometer - Earth Observing System (AMSR-E) instrument on the NASA Earth Observing System (EOS) Aqua satellite [*Wentz and Meissner*, 2004]. The data product is on a 0.25° grid at daily intervals. Since WB2 is near the coast, all the data there is flagged as bad and we use the nearest good location, -76° W 26.75° N.

One could also use sea-surface salinity data, for example from Aquarius or SMOS satellites. However the earliest of these time series only starts in 2009, so there is little overlap with the BPR data available at these sites.

2.1.3. Calculating steric pressure from mooring

To interpolate between instruments, we calculate reference profiles of temperature and salinity as functions of pressure, based on two piecewise cubic spline fits to the whole data series at that mooring. This is actually an easier calculation where moorings have collapsed causing instruments to vary in depth with time, as there are then more vertical sampling points. For salinity, the reference profile $S_{ref}(p)$ is defined from the minimum to maximum recorded pressure, p_{min} to p_{max}, and has spline break-points every 200 dbar to 2000 dbar, and every 500 dbar below. Therefore the reference profile near the surface is an extrapolation of the shallowest first cubic, but since the cubic spline is smooth at the breakpoints, carries information from deeper data too. There is a similar extrapolation near the sea-floor.

The reference profile is then removed from all the salinity data at a given time, say $S'(p,t) = S(p,t) - S_{ref}(p)$. Then we interpolate $S'(p,t)$ to regular (50 dbar) pressure intervals, p_{reg}, between the fixed pressures of the surface (p_{a_0}) and the ocean floor (p_{b_0}). The accuracy of this interpolation depends upon the vertical sampling as discussed below (§ 2.1.5). Various temporally varying profiles were investigated, but not found to improve the interpolation. Beyond the range of recorded pressures we use:

$$S'(p,t) = \begin{cases} S'(p_{min},t), & p_{a_0} < p_{reg} < p_{min}(t), \\ S'(p_{max},t), & p_{max}(t) < p_{reg} < p_{b_0}. \end{cases}$$

(A linear extrapolation was considered here but it is much more prone to very large errors.) We then replace the reference profile, $S(p_{reg},t) = S'(p_{reg},t) + S_{ref}(p_{reg})$.

For temperature we follow a similar procedure, removing a reference profile T_{ref} to give anomalies $T'(p, t)$, then interpolating to regular pressure intervals. However we will consider two cases: with and without SST data from satellite. Without SST, temperature is treated the same as salinity. When we use SST, we have an extra data point at the surface, $T'(p_a, t) = T(p_a, t) - T_{ref}(p_a)$, so do not need to extrapolate near the surface. We do not use SST to generate the reference profiles. Examples of S_{ref} and T_{ref} for EB1 are shown in figure 2.

Having derived a regular S and T profile at every timestep we use the equation of state to turn this into a regular density profile $\rho(p_{reg})$ at every timestep, and integrate to p_{tot} to give the changes in steric pressure.

2.1.4. Alternative method for interpolating S and T - using the Rapid standard calculation

A longer method for deriving steric pressure from the mooring in the Rapid project is described by *Johns et al.* [2005] and *Fillenbaum et al.* [1997]. This method uses the mean of stepped upwards and downwards projections of temperature (and similar for salinity) using gradients from climatology. We have tested this method as well, and found that it consistently gives slightly lower pressures than ours (for the case where we are not including the SST) by around 0.03 mbar (0.3 mm sea level). This is because their method of interpolation exaggerates curvature in the climatology reference profile, and will tend to underestimate temperature or salinity wherever $\mathrm{d}^2T/\mathrm{d}p^2 > 0$ or $\mathrm{d}^2S/\mathrm{d}p^2 > 0$. This occurs almost everywhere except above ~ 200 m and between $\sim 1100 - 1400$ m. We found that their method underestimates temperature compared to ours by an amount proportional to $\mathrm{d}^2T/\mathrm{d}p^2$. The effects on temperature and salinity to some extent cancel,

but overall lead to a slight underestimate of density. There is little effect on the time dependent calculation.

2.1.5. Vertical sampling error on the steric calculation

The accuracy of the density profile depends partly on the distribution of instruments down the mooring, particularly if there is sparse measurement of rapidly changing temperatures in the upper few hundred meters. The instrument distribution changes with new deployments, which may be at different nominal depths. It also changes during deployments due to a number of circumstances: when individual instruments fail; when a mooring is dragged out of position so that several instruments are temporarily displaced; and in one very bad case in 2005–6 when the WB2 mooring collapsed, and all instruments sank to below 2500 m.

To estimate the error that arises from the subsampling, we use the $1/4°$ NEMO global ocean model, run ORCA025-N206 [*Blaker et al.*, 2014]. There are up to 75 z-levels in the model, and sea-surface height on the free surface, and we extract time series of temperature and salinity at the nearest grid point to each mooring. We first calculate the steric height at each mooring using all the information. Then for every mooring time we check which NEMO depth levels are represented by the instruments currently providing data. This gives subsampled lists of depth levels, mimicking a mooring with these instruments. We recalculate the complete time series of steric height for each of these lists and find ϵ_m, the standard deviation of the error in the time series. In the plots that follow, we show $2\epsilon_m$, so 95% of results should fall within our error margin.

2.1.6. Effect of instrument error on the steric calculation

The mooring instruments themselves are subject to errors. The manufacturer's estimates of instrument accuracy for the moored CTDs used on the Rapid project are given in table 1. Additionally, calibrations against CTD casts may be carried out at deployment and/or recovery. If both are done, then linear instrument drifts can be corrected. The manufacturer also warns that changes in conductivity may not be linear, as errors on that sensor may be due to occasional fouling events on the mooring [*Sea-Bird Electronics*, 2015a].

The most obvious instrument error is the drift in their record of pressure, as illustrated in figure 3. Some of this drift may be due to actual change in depth of the instrument, in which case it should remain. This drift appears on almost all records on MAR1 and EB1, but not on WB2 or WB5. The drift appears to be fairly consistent with every deployment on EB1. It is negative (getting shallower), with a decaying exponential and linear part.

Kanzow et al. [2006] found that the MicroCAT CTDs at the Rapid array performed much better than the manufacturer's specifications. They calculated that *after linear drift correction*, the remaining error is typically (we assume this to mean 2σ) about 0.001 °C and 0.0002 S/m relative to the CTD reference casts. However, in practice often only one calibration is reported as having been done, and only constant offsets applied - either the pre or post deployment offset, or the mean of these. In a similar study on long-term behavior of MicroCAT CTDs in the Pacific, *Uchida et al.* [2008] found the maximum drifts of offsets to be 2 dbar/yr (at 4500 dbar), 0.001 C/yr and 0.0008 S/m/yr, with typical drifts of 1.2 dbar/yr, 0.0005 C/yr and 0.0008 S/m/yr. A year is a typical deployment length, and these numbers may reflect more realistic measurement errors.

The errors may not be independent, and errors in the pressure or temperature measured contribute to errors in the calculation of salinity (which is done at the BODC using the UNESCO 1983 equation of state). To derive the effect on the steric pressure of individual instrument errors, we run the calculation of the first deployment at EB1 repeatedly, with fixed errors applied to combinations of conductivity, temperature and pressure in turn. We test the case when all instruments on the mooring are biased in the same direction and when instruments have random errors. The results are summarized in table 1 — these numbers are summaries of calculations with the actual instrument spacing and realistic instrumental errors; dependence on depth and variability is complex and the numbers will vary in detail depending on these factors. Approximately half the error in steric pressure is attributable to the conductivity and half to the temperature, which also affects the salinity calculation. The error due to the instrument pressures is less severe, and if all the instruments on the mooring were underreading (too shallow) by 2 dbar (approx 2 m), we would overestimate density at a given depth, and hence overestimate the total steric pressure by around 0.5 mbar (approx 5 mm). This is the pure instrumental error for a realistic instrument distribution, the sampling error being accounted for separately.

In summary the most optimistic estimate of the error in steric pressure due to the instruments, assuming full calibration as described by *Kanzow et al.* [2006] and assuming instruments are randomly biased, is around $\epsilon_i = 0.15$ mbar (0.15 cm), 1σ. In practice it may be $\epsilon_i = 0.4$ mbar (0.4 cm) if each instrument's temperature and conductivity drift is independent, and over 1 mbar if they are correlated. This error assessment leads us to stress the importance of careful calibration at the start and end of each deployment if centimetric sea level accuracy is to be maintained over long time scales.

2.2. SSH from altimetry

We take the sea-surface height (SSH) from altimetry, specifically the Integrated Multi-Mission Ocean Altimeter Data for Climate Research TOPEX/Poseidon, Jason-1 and OSTM/Jason-2, [*Beckley et al.*, 2010, 2013]. The along-track TOPEX/Poseidon, Jason-1, and Jason-2/OSTM data has recently been reprocessed to take account of a number of orbital and sea-state bias corrections, and is available from the Physical Oceanography Distributed Active Archive Center (PO.DAAC). We use a version provided directly by Brian Beckley in which the inverse barometer/dynamic atmosphere correction is not applied, because this correction removes some high frequency ocean dynamic variability in addition to the inverse barometer correction. Figure 1 shows the position of the altimetry tracks nearest to the moorings. EB1 is positioned underneath the crossing point of two tracks. The individual along-track data points are recorded every 1 s and have a 10 day repeat rate - so there is data twice every 10 days for EB1. We normally use all data within a 0.125° range in latitude and longitude of the mooring, but for WB5 there is no data within 0.125° and we extend the range to 0.75°.

Much of the altimetry data is flagged as having possible errors. We reject all flagged data with one exception: for WB2 there is no data within a 0.5° range unless we accept flags 7 (Cross Track Distance >1 km) and 12 (Sigma 0 Ku Band Out of Range). With these flags we can use a radius of 0.125°.

2.2.1. Atmospheric pressure over the ocean

Since the altimetry has not been corrected for the inverse-barometer effect, we need to account for the atmospheric pressure also felt by the bottom pressure recorder. We

interpolate sea-level pressure from 6 hourly, 2.5° grid, NCEP/NCAR Reanalysis 1 [*Kalnay et al.*, 1996] onto the altimetry times and locations.

2.2.2. Tides in the altimetry data

Barotropic tides have been modeled and removed from the altimetry data, including the pole tide and other long period tides [*Beckley et al.*, 2013]. Internal tides that may exist in the steric signal are not removed by the altimetry processing, since they have wavelengths shorter than 200km at these latitudes [*Simmons et al.*, 2004]. At WB2, near the continental slope, it is possible that internal tides constrained to narrow vertical bands would be missed by the finite vertical sampling, an aspect of the vertical sampling error we are unable to test in the model.

2.3. Source of BP data

Bottom pressure data was also taken from the Rapid moorings. It was provided by BODC as integrated 10, 15, or 30 minute records. The data is provided as recorded (bpPS) and dedrifted (bpDR), where the drift is given by an exponential-plus-linear fit to the raw recorded data on each deployment. As we have previously argued [*Williams et al.*, 2014] this is not ideal, as there may be annual signals in the bottom pressure which cannot be adequately separated from an exponential-plus-linear instrument drift using a naïve fit. In the case of WB2, where there are overlapping bottom pressure records, bpDR contains discrepancies of up to 3 mbar (see figure 4). This is, for example, because the upwards drift that should be removed from the record ending in March 2008 coincides with the annual decline in BP from October 2007 to March 2008. The naïve fit thus misses this drift.

2.3.1. Improved dedrifting of bottom pressure data

The annual signal that exists in bottom pressure data can interfere with the correct removal of instrument drift [*Williams et al.*, 2014]. According to the methods detailed in that paper, we remove annual and other long period signals due to modeled ocean dynamics, the pole tide, other long period tides, the mean atmospheric pressure over the ocean, and the local influence of the annual signal in global ocean mass (amplitude 0.85 mbar peaking at 10 October). We then fit an exponential-plus-linear drift,

$$\text{drift} = a_1 + a_2(t - t_0)/30 + a_3 \mathrm{e}^{-(t-t_0)/(30a_4)},$$

to daily means of the residual, and it is this fit that we remove from the original bpPS record. For the nonlinear fit we use the function lsqcurvefit from the Matlab Optimisation Toolbox. To minimize floating-point errors from the exponent, we express the time as $(t - t_0)/30$, where t is time in days from t_0, 00:00 on the start date of the deployment. The coefficients to this fit, and the original fit found from bpDR-bpPS are provided in Supporting Information.

This procedure somewhat improves the characterization of drift, as can be seen from the closer overlap of neighboring instruments (figure 4). In particular, at EB1 there is better agreement between records 946112 and 946148 (red and yellow curves) in late 2007, and between all records in early 2008. However there is less agreement between records in late 2008. The records 945944 and 945956 (blue and green curves) in 2005 have no overlap with other records but the new instrument drift removal leaves a low frequency signal not present in the original dedrifted record. This could be an example of an annual signal incorrectly removed by the original dedrifting. At MAR1 there is an improvement at the beginning of the overlap in 2008 but worsening agreement by the end of the year. WB2 shows the greatest improvement, with improved agreement between concurrent records

946204 and 946216 (blue and green) in mid-2005, improved overlap between them and the following two records in 2006, and very much improved agreement with the final overlap in 2007-8.

2.3.2. Tide removal

After dedrifting, we remove monthly and higher frequency tides from the BPR data using an updated form of the TIRA software [*Murray*, 1964], fitting 60 major harmonic constituents. This empirical fit may differ slightly from the GOT4.8 tidal model used to remove high frequencies from the altimetry data. We cannot use the (more accurate) tides derived from BP measurements to correct the altimetry, because BP also records the tidal motion of the sea floor. For the altimetry, we choose therefore to use the best tidal fit determined using altimeter data, which is supplied with the altimeter product. Being tuned to represent the barotropic tide only, this leaves any baroclinic tide in the sea level, where it will be compensated by the measured steric component. We also model and remove the pole tide and other long-period (> 1 month) tides, using a self-consistent equilibrium tidal calculation as in *Williams et al.* [2014].

2.4. Assumption of no vertical crustal movement

In practice, in addition to ocean dynamics, bottom pressure recorders measure water column variations caused by both crustal motion and changes in the geoid. However, the steric-plus-altimetry system does not observe crustal motion, only changes in the geoid. Thus, to understand the level of disagreement that this may introduce in the comparison between these methods of measuring bottom pressure, we need an estimate of $H'(t)$ (vertical crustal motion) for equation 6. Crustal motion can be caused by a number of processes, such as earthquakes, sediment loading, glacial isostatic adjustment

(GIA), and the annual hydrological cycle. We consider estimates for the last two. For GIA, we examine the results of *Tamisiea* [2011], which used a modified ICE-5G ice history [*Peltier*, 2004] and the VM2 earth model [*Peltier*, 1996], and explore the range of model predictions resulting from varying the Earth parameters. Moorings WB2 and WB5 are near the US East coast, and thus are likely subsiding (approximately 1 mm/yr, with a similar uncertainty estimated from the variation of earth model parameters) due to the collapse of the forebulge of Laurentian ice sheet. The subsidence at EB1 and MAR1 is likely of order 0.5 mm/yr. To find the the annual variation in H', arising from elastic response to the annual water cycle, we follow *Williams et al.* [2014]. In particular, we examine the crustal deformation resulting from the hydrological and atmospheric loading (and corresponding ocean load) detailed in Section 4.2 and the ocean dynamics described in Section 2.1.5. The annual amplitude is around 1–2 mm at the Rapid sites.

If one were designing a mooring to explicitly measure the change in ocean mass (e.g. *Hughes et al.* [2012], *Williams et al.* [2014]), then when choosing a site one would have to have to carefully consider the GIA contribution, as the crustal motion can be significant even in the far field. While one might typically consider the relative sea level change due to GIA to be small in the far field, this is partially due to the cancellation of geoid and crustal motion changes. For this comparison of BP from BPRs and from steric-plus-altimetry, the error due to neglecting vertical crustal movement is smaller than that due to other causes, such as the conductivity measurement.

3. Results

3.1. Reconstruction of bottom pressure

Figures 5–8 show how well we can reproduce the bottom pressure using steric signal and altimetry, for each of the moorings. In the middle panels (b,c) the heavy black line shows the bottom pressure measurement, detided and dedrifted as described in § 2.3.1. The range in the dedrifting, where overlapping bottom pressure records do not coincide, is shown with grey bars; the black line being the mean of overlapping records. Vertical offsets on both curves are arbitrary and any true trend has been removed from the measured BP curve by the dedrifting procedure.

The green line shows our prediction for bottom pressure based on the steric signal calculated from the temperature and salinity measured at the mooring, plus sea-surface height from altimetry, and corrections for long-period tides and global atmosphere as described above. SSH is the average of all altimetry data available within 0.125° range (0.75° for WB5) of the mooring. The width of the yellow error band is $2\epsilon_m$, the time-varying error due to the vertical sampling of the instruments on the mooring, and the green band is $2\epsilon_i$, the constant errors due to the instruments.

Panel (a) of figures 5–8 shows the altimetry signal at nearby track points (light blue lines) and the mean of these (dark blue). The spread of results in this panel gives an idea of altimetric uncertainties when the sampling position is sufficiently close to the mooring. Note that our error estimates represent only the error in the steric sea level, and exclude any error in the altimetry.

On both MAR1 and EB1 the SSH has greater variability than BP, both recorded and constructed. This can be seen by comparing the panels (a) and (c) of figures 5–6.

Panel (d) of figures 5–8 shows the measured and nominal pressure at each CTD instrument on the mooring. Colors in this panel and vertical lines on all panels indicate changes in the number of working instruments, and gaps can be seen where the mooring suffered collapses or multiple instrument failures.

3.1.1. Vertical sampling error

For most times, the error band predicted by the model, based on the number and depth of instruments, is accurate, and our prediction for the pressure falls within $2(\epsilon_m + \epsilon_i)$ of the recorded pressure. ϵ_i is constant, but ϵ_m varies from 0.03 to 19 cm. It is typically about 1 cm. For example at mooring EB1 (figure 5) in late 2006 several instruments failed, and there is a sudden increase in the predicted error ϵ_m and in the disagreement observed between our prediction and the measured bottom pressure.

The greatest density fluctuations occur near the surface, and using the sea-surface temperature reduces ϵ_m by about 50% in most cases, with greatest benefit occurring when there are no shallow instruments. There is a corresponding improvement in the prediction of bottom pressure, for example in April 2007 at EB1, when the shallowest instrument is at around 118 m, disagreement reduces from around 2.5 cm to 1 cm.

We also tested in certain cases how much the vertical sampling error would be reduced by using extra instruments near the surface. Suppose the sampling were 16 instruments spaced as at WB5 in 2005–9, with the shallowest instrument at 80 m, and using satellite SST. Then ϵ_m=[0.7, 0.8, 1.3, 1.5] cm at [EB1, MAR1, WB5, WB2]. The addition of an extra instrument at 20 m reduces the vertical sampling error to [0.6, 0.8, 0.9, 0.9] cm, the greatest benefit being at the western boundary. Without SST the benefit of an additional

instrument at 20 m is greater, improving ϵ_m from [2.2, 2.1, 3.2, 2.9] cm to [0.6, 0.7, 0.8, 0.9] cm.

3.1.2. Effect of SST

Using SST generally reduces the mismatch between measured and reconstructed BP, particularly at EB1 and MAR1, though there is little or no improvement when the mooring reaches close to the surface, as in 2009. Using SST brings less improvement to the predictions at WB2 than for the other records. This may be because the nearest satellite SST measurement to WB2 is at 76.125W, 26.51N, 0.6° (60 km) from the mooring. Surface temperature at the corresponding position in the model is used in calculating the green error bar shown. For the 2008-9 deployment at WB2 the shallowest instrument on the mooring is $\sim$ 60 m, and the predicted BP fits well.

We tested in the NEMO model whether using surface salinity from satellites would bring any benefit, and found that it did not improve the vertical sampling error ϵ_m at these mooring sites.

3.1.3. Problems with reconstruction of BP

There are times for which $2(\epsilon_m + \epsilon_i)$ is not sufficient to explain the differences between recorded bottom pressure and that calculated from the mooring. April 2008 at EB1 is an example of this. $\epsilon_m = 1.2$ cm, and $\epsilon_i = 0.4$ cm but discrepancies of over 6 cm are seen.

For WB5, we only have a short period of bottom pressure data available, in 2005. The results of the steric + SSH reconstruction are poor, with very high variability not seen in the bottom pressure record. SSH is highly variable in this area, and the distance to the altimetry track is one possible cause of the discrepancy. Comparison of SSH timeseries in the NEMO global ocean model suggests that this only accounts for less than 5 cm of the

difference, but according to the 1/12° OCCAM global ocean model this could account for around 10 cm difference, and according to the AVISO gridded product 8 cm. The spread of the recorded altimetry is also particularly large in 2005, as seen in figure 7(a).

3.2. Time required to derive a trend

So far we have removed trends in order to compare the BPR and reconstructed BP data. Now we consider whether it is possible to detect a trend in the reconstructed BP.

3.2.1. Estimate from spectrum of signal

Even with perfect measurements, the time required to distinguish a trend from variability in a signal depends on the spectrum of the signal. *Hughes and Williams* [2010] showed that the time required to determine a 1 mm/yr trend in sea-level from altimetry data is around [10, 10, 20, 20] years at [EB1, MAR1, WB5, WB2]. Applying the same technique to the NEMO 1/4° model we find that a 1 mm/yr trend in SSH can only be distinguished in slightly longer [15, 18, 27, 21] years at [EB1, MAR1, WB5, WB2]. In the model we can switch from looking at sea-level to bottom pressure, and the same trend in bottom pressure can be seen in only around 5 years at all four mooring locations.

3.2.2. Estimate from trends fitted to samples

There is a method to provide an approximate time required to detect a trend that is simpler than that of *Hughes and Williams* [2010], and which can be applied both to the model and to the irregular real data. We assume a measurement campaign of N days. We take 100 uniformly-spaced (and overlapping) samples of N days from the steric pressure time series, and to each of these add an instrument error function. Then we fit a trend to each N-day section, arriving at a wide range of trends (for example between -20 mm/yr and 20 mm/yr for $N = 200$). We then repeat this with N varying from 100 days up

to half the length of the model timeseries. As the timeseries get longer, the calculated trends will gradually converge on the trend fitted to the entire timeseries. We look for the sample length required for all of the trends fitted to be within ± 1 mm/year of the actual trend in the model data. Figure 9 (upper panel) illustrates the convergence of trends in the model at EB1. The range of trends converges approximately according to $N^{-3/2}$, roughly consistent with white noise [*Williams*, 2003], although after about 10 years the convergence is slower.

Based on this method (using the NEMO model), if it were possible to make a single continuous timeseries measurement with no instrument errors, and no error introduced from vertical sampling, the minimum time to detect a ± 1 mm/year trend in bottom pressure with 95% of measurement campaigns would be [8,8,13,8] years at [EB1, MAR1, WB5, WB2]. These theoretical figures are slightly longer than the above estimates using the technique of *Hughes and Williams* [2010].

3.3. Effect of measurement error on time to detect trend

If instruments were calibrated at the beginning and end of every deployment, to constrain errors as described by *Kanzow et al.* [2006], and assuming that instrument errors are independent, then the steric pressure error due to instruments is around 0.01 mbar (1σ (due to instrument resolution) at the beginning and end of the deployments and around 0.15 mbar within it. We model this as a quadratic error with standard deviation 0.15mbar maximum extent for each deployment. Then 95% of continuous measurement campaigns of [10,12,16,12] years at [EB1, MAR1, WB5, WB2], with 16 instruments distributed as at the WB5 mooring from 2006 onward, and redeployed annually, would be able to detect a trend to an accuracy of ± 1 mm/year.

As indicated in the processing logs of the BODC metadata reports, in some cases the instruments were in practice only calibrated at the beginning or end of every deployment. Some instruments were calibrated at both, but only the mean of the two offsets was removed, not a linear trend. In this cases there would be added to the instrument error a drift, as derived from the measurements by *Uchida et al.* [2008], leading to steric pressure drift of around 0.5 mbar/yr. We model this as an additional linear error for each deployment. Then 95% of continuous measurement campaigns of [12,12,17,12] years at [EB1, MAR1, WB5, WB2], with 16 instruments distributed as at the WB5 mooring, and redeployed annually, would be able to detect a trend to an accuracy of ± 1 mm/year. This is the case illustrated in figure 9.

The same technique can be applied to the BP signal constructed from data, this time using the sampling error ϵ_m changing in time as we have estimated (figure 9, lower panel). The increased ϵ_m during some deployments increases the time required to detect a given trend, but the convergence for short measurement campaigns is similar to that for the model. We estimate that if the current measurement campaign were to continue with similar quality, a trend with an accuracy of 1 mm/yr should be detectable at EB1 by around 2019.

These figures do not include uncertainties in trend introduced by the satellite SST or the altimetry, which should be added to the 1 mm/yr. Altimetry is dependent on careful calibration of many parameters, the subject of close analysis by many authors. For example *Ablain et al.* [2015, figure 7] showed that the calculation of mean sea-level by Envisat is adjusted by 0.8 mm/yr by the latest altimeter corrections.

4. Conclusions

Our purpose was to determine whether data from tall moorings can provide a sufficiently accurate constraint on the steric component of sea level variability to allow for a measurement of deep ocean bottom pressure variability. Such a measurement would not be subject to the problems of drift or of datum loss between deployments which limit the capability of present BPRs.

We identified two main error sources in this steric sea level determination: sampling error and instrument error. Both can be important at the mbar (cm) level, and we found that it is particularly important to have good sampling near the surface, including in the mixed layer. In the absence of near-surface instruments, sea-surface temperature measurements from satellite could reduce the sampling error. Salinity uncertainties contribute most to the instrument-related error in steric sea level, with both conductivity and temperature uncertainties contributing to the salinity error. The pressure drift of CTD instruments on the mooring is acceptable for this reconstruction, as is the tendency of moorings to fluctuate in depth when dragged out of position. Even collapsed moorings can provide some useful data, with predictable if larger error margins.

Using data from four North Atlantic moorings in the Rapid array, we showed that a combination of these error estimates was sufficient to account for the observed mismatch between bottom pressure and (IB-corrected sea level) minus (steric sea level) variability at most times, though the mismatch was larger at site WB5 where the distance to the nearest altimeter track was greater, and introduced an extra source of error of around 10 mbar (cm). This analysis validated the use of NEMO model data as a means of assessing the sampling error. For periods of good vertical sampling we find a sampling error (1σ) of

below 1 mbar (cm). With a typical mooring configuration, we find that the practice of using a single calibration at the start or end of a deployment can increase the instrument error significantly, from about 0.15 to 0.4 mbar (cm) if the instrument calibration errors are random. These errors can be about four times larger if they are perfectly correlated.

Finally, we used the model data to simulate realistic sampling and instrumental errors, as well as ocean dynamical signals, in order to assess the time necessary to detect a linear trend of 1 mm/year on top of this stochastic variability, with 95% confidence. For the eastern Atlantic, where dynamical variability is weaker than the west, and with optimal deployment practice as described by *Kanzow et al.* [2006], we find that such a trend could be measured after approximately 10 years. While this is longer than the 8 years which would be necessary given perfect BP measurements, it is still shorter than the 15-25 years required for perfectly-measured sea level.

5. Discussion

Past studies similar to ours have usually focused on the issue of reconstructing the relatively large sea level signal from a combination of the small BP variability and some measure of steric variability, rather than on determining the BP variability. *Behnisch et al.* [2013] combined acoustic travel time with climatological hydrography to infer the steric signal, and added this to BP measurements south and west of South Africa to produce sea level predictions to compare with altimetry. Their error estimate for the steric signal is 4.53 cm, larger than ours which has the advantage of full temperature and salinity measurements. However, it is quite plausible that the integral nature of the acoustic travel time measurement would help reduce sampling errors if used in combination with data from a tall mooring.

Picaut et al. [1995] performed a short study similar to ours in the equatorial Pacific, as part of verification of the satellite altimetry, but did not use the direct bottom pressure measurement they took because they judged the drift to be too large (though they did use the data for tidal calculation). Based on 6 months of data with very good resolution near the surface, and with 18 CDT casts available to test the instrumental errors (which they estimated to be below 1 cm), they estimated rms total errors on the steric signal of 1.1 cm at one site and about 1.5 cm at a second site, the largest contribution being from vertical sampling. Based on our assessment, this is close to being as good as it is possible to achieve. Their instantaneous comparisons with altimetry achieved an overall error of about 3.5 cm, which could be reduced to a little under 2 cm by low pass filtering in time and taking advantage of the large length scales of the equatorial dynamics to average the altimeter data (though this includes only a narrow spectral band from 2–6 month period).

A good rule of thumb thus appears to be that optimal mooring data can provide the steric signal at a single point with an accuracy of 1–2 cm. As a means of determining bottom pressure variability, this has some advantages and some disadvantages over other methods.

Satellite gravity from GRACE and from currently-foreseeable missions appears to do a very good job at large spatial scales, but shorter length scales such as the continental slope width are likely to remain out of range for some time [e.g. *Panet et al.*, 2013], and such complex systems still need independent verification, particularly as they rely on geophysical models and subtle combinations of data types to account for solid earth variability and degree 1 and 2 spherical harmonic components.

The combination of altimetry and Argo data, as used by *Chambers and Willis* [2010] among others achieves an accuracy of about 2 cm on bottom pressure as compared to GRACE. This is comparable to the error from a single mooring, but relies again on large scale spatial averaging. An individual Argo profile cannot be as well calibrated as an annually-serviced mooring, and the present Argo network only samples to depths of 2000 m. There is clearly a trade off between the number of profiles (effectively spatial averaging) and completeness/instrumental error in this case.

In some ways the ideal measurement would be a direct time series of BP from the sea floor. Even if this could be obtained without BPR instrumental drift, it would suffer from one problem which the mooring and Argo methods do not suffer from: any local sea floor motion would contaminate the signal, making the measurement unrepresentative of the large scales. This influence is absent from the altimetry + steric method.

On the other hand, this absence means that we rely on geophysical models of the large scale motions of the sea floor to relate the measurement to true bottom pressure, and hence to the mass component of sea level. We also have the disadvantage of relying on satellite altimeter measurements, which have their own complex error sources [e.g. *Ablain et al.*, 2015].

Thus, while all methods of monitoring BP variability have shortcomings, the use of tall moorings plus altimetry has a valuable place, particularly on time scales of order 10–20 years.

References

Ablain, M., A. Cazenave, G. Larnicol, M. Balmaseda, P. Cipollini, Y. Faugère, M. J. Fernandes, O. Henry, J. A. Johannessen, P. Knudsen, O. Andersen, J. Legeais, B. Meyssignac, N. Picot, M. Roca, S. Rudenko, M. G. Scharffenberg, D. Stammer, G. Timms, and J. Benveniste (2015), Improved sea level record over the satellite altimetry era (1993–2010) from the climate change initiative project, *Ocean Science*, *11*(1), 67–82, doi:10.5194/os-11-67-2015.

Beckley, B., R. Ray, S. Holmes, N. Zelensky, F. Lemoine, X. Yang, S. Brown, S. Desai, G. Mitchum, and J. Hausman (2013), *Integrated Multi-Mission Ocean Altimeter Data for Climate Research TOPEX/Poseidon, Jason-1 and OSTM/Jason-2. User's Handbook version 2*, California Institute of Technology.

Beckley, B. D., N. P. Zelensky, S. A. Holmes, F. G. Lemoine, R. D. Ray, G. T. Mitchum, S. D. Desai, and S. T. Brown (2010), Assessment of the Jason-2 extension to the TOPEX/Poseidon, Jason-1 sea-surface height time series for global mean sea level monitoring, *Marine Geodesy*, *33*(sup1), 447–471, doi:10.1080/01490419.2010.491029.

Behnisch, M., A. Macrander, O. Boebel, J.-O. Wolff, and J. Schrter (2013), Barotropic and deep-referenced baroclinic SSH variability derived from Pressure Inverted Echo Sounders (PIES) south of Africa, *Journal of Geophysical Research: Oceans*, *118*(6), 3046–3058, doi:10.1002/jgrc.20195.

Bingham, R. J., and C. W. Hughes (2008), Determining North Atlantic meridional transport variability from pressure on the western boundary: A model investigation, *Journal of Geophysical Research-Oceans*, *113*(C9), doi:10.1029/2007JC004679.

Blaker, A., J.-M. Hirschi, G. McCarthy, B. Sinha, S. Taws, R. Marsh, A. Coward, and B. de Cuevas (2014), Historical analogues of the recent extreme minima observed in the Atlantic meridional overturning circulation at 26°N, *Climate Dynamics*, pp. 1–17, doi:10.1007/s00382-014-2274-6.

Chambers, D. P., and J. K. Willis (2010), A global evaluation of ocean bottom pressure from GRACE, OMCT, and steric-corrected altimetry, *J. Atmos. Oceanic Technol.*, *27*(8), 1395–1402.

Chereskin, T. K., K. A. Donohue, and D. R. Watts (2012), cDrake: Dynamics and transport of the Antarctic Circumpolar Current in Drake Passage, *Oceanography*, *25*(3), 134–135, doi:10.5670/oceanog.2012.86.

Elipot, S., E. Frajka-Williams, C. W. Hughes, and J. K. Willis (2013a), The observed North Atlantic Meridional Overturning Circulation: its meridional coherence and ocean bottom pressure, *J. Phys. Oceanogr.*, *44*(2), 517–537.

Elipot, S., C. Hughes, S. Olhede, and J. Toole (2013b), Coherence of western boundary pressure at the RAPID WAVE array: boundary wave adjustments or deep western boundary current advection?, *J. Phys. Oceanogr.*, *43*(4), 744–765, doi:10.1175/JPO-D-

12-067.1.

Fillenbaum, E. R., T. N. Lee, W. E. Johns, and R. J. Zantopp (1997), Meridional heat transport variability at 26.5°N in the North Atlantic, *J. Phys. Oceanogr.*, *27*(1), 153–174.

Hirschi, J., J. Baehr, J. Marotzke, J. Stark, S. Cunningham, and J.-O. Beismann (2003), A monitoring design for the atlantic meridional overturning circulation, *Geophysical Research Letters*, *30*(7), n/a–n/a, doi:10.1029/2002GL016776.

Howe, P. J., K. A. Donohue, and D. R. Watts (2009), Stream-coordinate structure and variability of the kuroshio extension, *Deep Sea Research Part I: Oceanographic Research Papers*, *56*(7), 1093 – 1116, doi:10.1016/j.dsr.2009.03.007.

Hughes, C., and B. de Cuevas (2001), Why western boundary currents in realistic oceans are inviscid: A link between form stress and bottom pressure torques, *Journal of Physical Oceanography*, *31*(10), 2871–2885.

Hughes, C. W., and S. D. P. Williams (2010), The color of sea level: Importance of spatial variations in spectral shape for assessing the significance of trends, *Journal of Geophysical Research-Oceans*, *115*, C10,048, doi:10.1029/2010JC006102.

Hughes, C. W., M. P. Meredith, and K. J. Heywood (1999), Wind-driven transport fluctuations through Drake Passage: a southern mode, *J. Phys. Oceanogr.*, *29*(8), 1971–1992.

Hughes, C. W., M. E. Tamisiea, R. J. Bingham, and J. Williams (2012), Weighing the ocean: Using a single mooring to measure changes in the mass of the ocean, *Geophysical Research Letters*, *39*(17), L17,602, doi:10.1029/2012GL052935.

Hughes, C. W., S. Elipot, M. . Morales Maqueda, and J. W. Loder (2013), Test of a method for monitoring the geostrophic Meridional Overturning Circulation using only

boundary measurements, *J. Atmos. Oceanic Technol.*, *30*(4), 789–809.

Johns, W. E., T. Kanzow, and R. Zantopp (2005), Estimating ocean transports with dynamic height moorings: An application in the Atlantic Deep Western Boundary Current at 26°N, *Deep Sea Research Part I: Oceanographic Research Papers*, *52*(8), 1542 – 1567, doi:10.1016/j.dsr.2005.02.002.

Kalnay, E., M. Kanamitsu, R. Kistler, W. Collins, D. Deaven, L. Gandin, M. Iredell, S. Saha, G. White, J. Woollen, Y. Zhu, M. Chelliah, W. Ebisuzaki, W. Higgins, J. Janowiak, K. Mo, C. Ropelewski, J. Wang, A. Leetmaa, R. Reynolds, R. Jenne, and D. Joseph (1996), The NCEP/NCAR 40-year reanalysis project, *Bulletin Of The American Meteorological Society*, *77*(3), 437–471.

Kanzow, T., U. Send, W. Zenk, A. D. Chave, and M. Rhein (2006), Monitoring the integrated deep meridional flow in the tropical north atlantic: Long-term performance of a geostrophic array, *Deep Sea Research Part I: Oceanographic Research Papers*, *53*(3), 528 – 546, doi:10.1016/j.dsr.2005.12.007.

Meredith, M. P., P. L. Woodworth, T. K. Chereskin, D. P. Marshall, L. C. Allison, G. R. Bigg, K. Donohue, K. J. Heywood, C. W. Hughes, A. Hibbert, A. M. Hogg, H. L. Johnson, L. Jullion, B. A. King, H. Leach, Y.-D. Lenn, M. A. Morales Maqueda, D. R. Munday, A. C. Naveira Garabato, C. Provost, J.-B. Salle, and J. Sprintall (2011), Sustained monitoring of the Southern Ocean at Drake Passage: past achievements and future priorities, *Reviews of Geophysics*, *49*(4), doi:10.1029/2010RG000348.

Murray, M. (1964), A general method for the analysis of hourly heights of the tide., *International Hydrographic Review*, *41*(2), 91–101.

Panet, I., J. Flury, R. Biancale, T. Gruber, J. Johannessen, M. van den Broeke, T. van Dam, P. Gegout, C. Hughes, G. Ramillien, I. Sasgen, L. Seoane, and M. Thomas (2013), Earth system mass transport mission (e.motion): A concept for future earth gravity field measurements from space, *Surveys in Geophysics*, *34*(2), 141–163, doi:10.1007/s10712-012-9209-8.

Peltier, W. (2004), Global glacial isostasy and the surface of the ice-age earth: the ICE-5G (VM2) model and GRACE, *Annual Review of Earth and Planetary Sciences*, *32*(1), 111–149, doi:10.1146/annurev.earth.32.082503.144359.

Peltier, W. R. (1996), Mantle viscosity and ice-age ice sheet topography, *Science*, *273*(5280), 1359–1364, doi:10.1126/science.273.5280.1359.

Picaut, J., A. J. Busalacchi, M. J. McPhaden, L. Gourdeau, F. I. Gonzalez, and E. C. Hackert (1995), Open-ocean validation of topex/poseidon sea level in the western equatorial pacific, *Journal of Geophysical Research: Oceans*, *100*(C12), 25,109–25,127, doi: 10.1029/95JC02128.

Polster, A., M. Fabian, and H. Villinger (2009), Effective resolution and drift of paroscientific pressure sensors derived from long-term seafloor measurements, *Geochemistry, Geophysics, Geosystems*, *10*(8), Q08,008, doi:10.1029/2009GC002532.

Ray, R. D. (2013), Precise comparisons of bottom-pressure and altimetric ocean tides, *Journal of Geophysical Research: Oceans*, *118*(9), 4570–4584, doi:10.1002/jgrc.20336.

Rayner, D., J. J.-M. Hirschi, T. Kanzow, W. E. Johns, P. G. Wright, E. Frajka-Williams, H. L. Bryden, C. S. Meinen, M. O. Baringer, J. Marotzke, L. M. Beal, and S. A. Cunningham (2011), Monitoring the Atlantic meridional overturning circulation, *Deep Sea Research Part II: Topical Studies in Oceanography*, *58*(17–18), 1744–1753, doi:

10.1016/j.dsr2.2010.10.056, climate and the Atlantic Meridional Overturning Circulation.

Sea-Bird Electronics (2015a), SBE 37-SMP MicroCAT C-T (P) Recorder, FAQ, *Tech. rep.*, accessed 5 Feb 2015.

Sea-Bird Electronics (2015b), MicroCAT C-T Recorder SBE 37-SMP Data Sheet, *Tech. rep.*, 1808 136th Place NE, Bellevue, Washington 98005 USA, accessed 5 Feb 2015.

Simmons, H. L., R. W. Hallberg, and B. K. Arbic (2004), Internal wave generation in a global baroclinic tide model, *Deep Sea Research Part II: Topical Studies in Oceanography*, *51*(25–26), 3043–3068, doi:http://dx.doi.org/10.1016/j.dsr2.2004.09.015, small and mesoscale processes and their impact on the large scale.

Tamisiea, M. E. (2011), Ongoing glacial isostatic contributions to observations of sea level change, *Geophysical Journal International*, *186*(3), 1036–1044, doi:10.1111/j.1365-246X.2011.05116.x.

Uchida, H., T. Kawano, and M. Fukasawa (2008), In situ calibration of moored ctds used for monitoring abyssal water, *J. Atmos. Oceanic Technol.*, *25*(9), 1695–1702.

Vinogradova, N. T., R. M. Ponte, and D. Stammer (2007), Relation between sea level and bottom pressure and the vertical dependence of oceanic variability, *Geophys. Res. Lett.*, *34*(3), L03,608–, doi:10.1029/2006GL028588.

Wahr, J., D. A. Smeed, E. Leuliette, and S. Swenson (2014), Seasonal variability of the red sea, from satellite gravity, radar altimetry, and in situ observations, *Journal of Geophysical Research: Oceans*, *119*(8), 5091–5104, doi:10.1002/2014JC010161.

Watts, D. R., and H. Kontoyiannis (1990), Deep-ocean bottom pressure measurement: drift removal and performance, *Journal of Atmospheric and Oceanic Technology*, *7*(2),

Figure 1. Mooring positions and altimetry data points nearby the moorings WB2, WB5, MAR1 and EB1. Background is standard deviation of bottom pressure from the NEMO 1/12 degree global ocean model, with depth contours. Pink rectangles correspond to the extent of altimetry data.

Figure 2. Reference profiles for temperature, $T_{ref}(p)$, (left) and salinity, $S_{ref}(p)$, (right) for mooring EB1. Blue dots are all of the recorded CTD data, red dots are the SST data.

Figure 3. Examples of instrument pressure drift on part of the EB1 mooring. Dashed lines indicate nominal pressure of each instrument. Colors change with any change in the number of working instruments. Instruments deployed at greater depth exhibit similar drifts.

296–306, doi:10.1175/1520-0426(1990)007¡0296:DOBPMD¿2.0.CO;2.

Watts, D. R., X. Qian, and K. L. Tracey (2001), Mapping abyssal current and pressure fields under the meandering Gulf Stream, *J. Atmos. Oceanic Technol.*, *18*(6), 1052–1067.

Wentz, F., and T. Meissner (2004), Amsr-e/aqua daily l3 global ascending/descending .25x.25 deg ocean grids. version 2, ae dyocn., *Boulder, Colorado USA: National Snow and Ice Data Center.*

Williams, J., C. W. Hughes, M. E. Tamisiea, and S. D. P. Williams (2014), Weighing the ocean with bottom-pressure sensors: robustness of the ocean mass annual cycle estimate, *Ocean Science*, *10*(4), 701–718, doi:10.5194/os-10-701-2014.

Williams, S. D. P. (2003), The effect of coloured noise on the uncertainties of rates estimated from geodetic time series, *Journal of Geodesy*, *76*(9-10), 483–494, doi:10.1007/s00190-002-0283-4.

Figure 4.   Top panel: WB2 with dedrifting as provided, 2007-8, with 5 day running average. Despite high-frequency correlation, the record 946228 (yellow) that starts in April 2007 is around 0.03 dbar (3 cm) higher than that in 946289 (black). By the end of the overlap in April 2008 it is 0.02 dbar (2 cm) lower. Lower panels: Anomaly from mean of bottom pressure measurements at four moorings after dedrifting as provided, and with dedrifting as described in § 2.3.1. For clarity, calendar monthly means (omitting months with < 20 days of data) are plotted. Colors indicate BPR deployments.

Figure 5.   Quality of reconstruction of recorded bottom pressure at EB1. Caption overleaf.

Figure 5.   (continued)

Panel (a): SSH (cm) from altimetry points within a radius of 0.125° of EB1 (light blue) and their mean (dark blue). Panels (b,c): Bottom pressure anomalies (mbar) as recorded and detided (black, grey bar indicates range of overlapping deployments), and as constructed from steric from CTD mooring and SSH from altimetry (dark green) at EB1. The steric calculation is done (b) without, (c) with, SST from satellite. The green ribbon shows $\epsilon_i = 2$ mbar, to illustrate the steric instrument errors, and the yellow ribbon shows the additional error ϵ_m varying in time according to the vertical sampling on the mooring. Top three panels are monthly averages of data at the altimetry times. Panel (d): nominal and recorded pressures (dbar, approximately depth in m) of the instruments on the CTD mooring, original times. Colors in this panel and vertical lines indicate changes in the number of working instruments on the mooring.

Figure 6.   As figure 5, mooring MAR1.

Figure 7. As figure 5, mooring WB5.

Figure 8. As figure 5, mooring WB2.

Figure 9. Range of trends fitted to samples of increasing length, representing N-day measurement campaigns from: (upper panel) the NEMO 1/4 model at EB1, subsampled and with noise to mimic 16 instruments calibrated only at the beginning of deployments; and (lower panel) the reconstructed bottom pressure signal with actual sampling error and ϵ_i as above. Crosses indicate the mean trend of samples, vertical lines the range of 90%, 95% and 100% of samples. In both cases the trend over the entire record has first been fitted and subtracted. Also shown is $\pm cN^{-3/2}$, for arbitrary c.

Table 1. Errors on instruments and subsequent calculations. We assume "typical" to be 2σ, and quote ϵ_i as σ.

	Conductivity	Temperature	Pressure % of full	Effect on steric pressure, ϵ_i all instr.	random
	S/m	°C	scale range	mbar ($\approx$ cm)	mbar ($\approx$ cm)
Initial accuracy[a]	0.0003	0.002	0.1%	1	0.25
Stability, /year[a]	0.0036	0.0024	0.05%	8	2.3
Resolution[a]	0.00001	0.0001	0.002%	0.04	0.01
Typical error after calibration[b]	0.0002	0.001	2 dbar	0.7	0.15
Typical stability, /year[c]	0.0008	0.001	0.03%	1.3	0.4

[a] *Sea-Bird Electronics* [2015b], [b] *Ka*
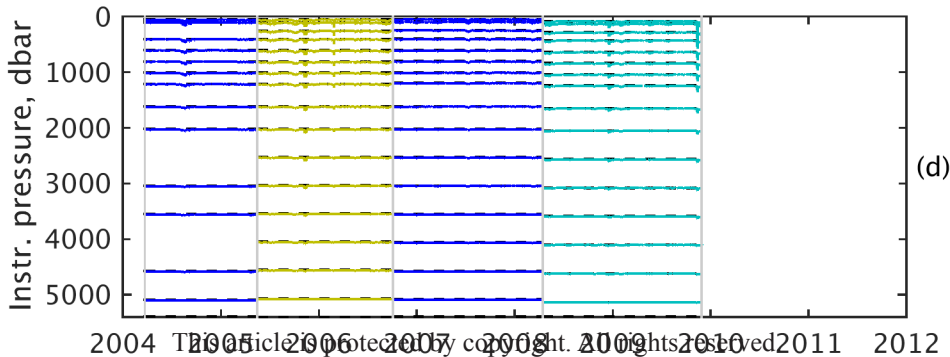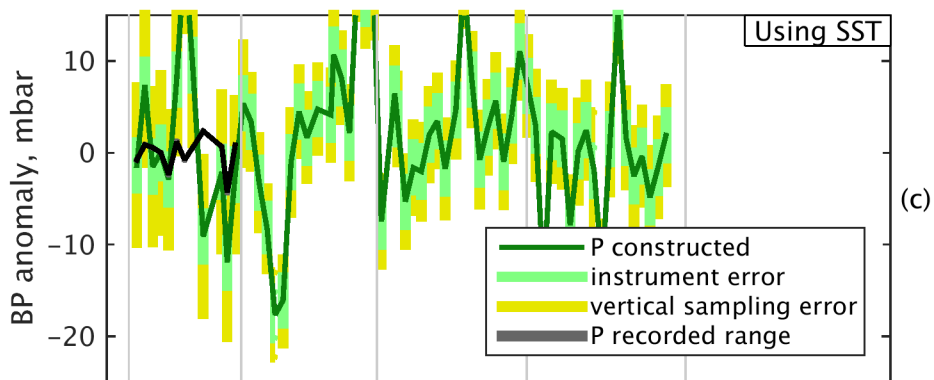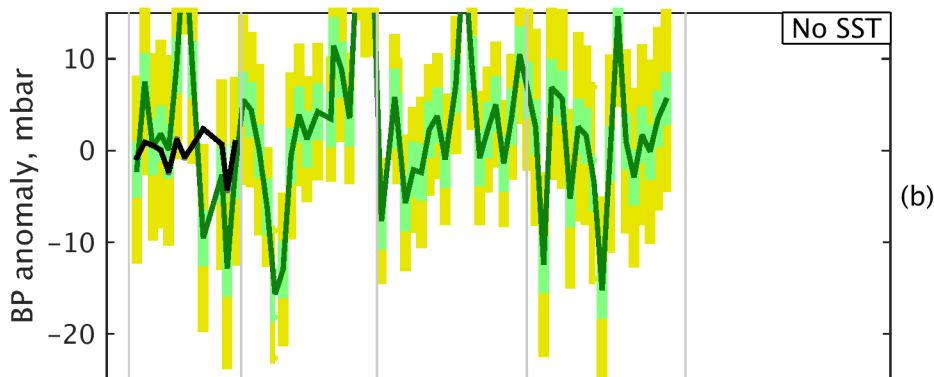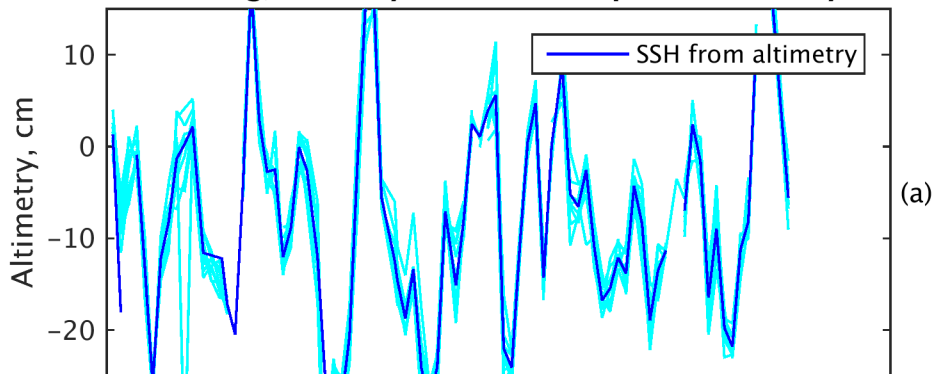
[c] *Uchida et al.* [2008].
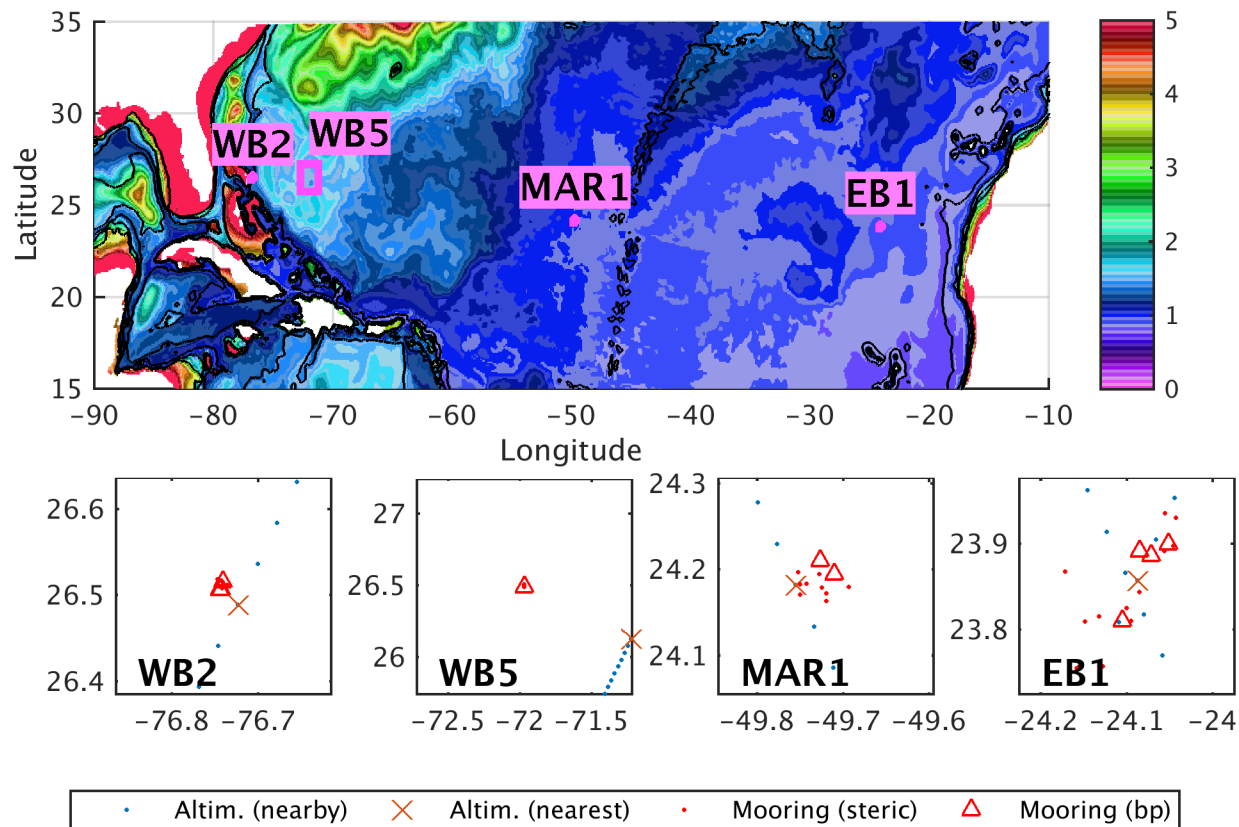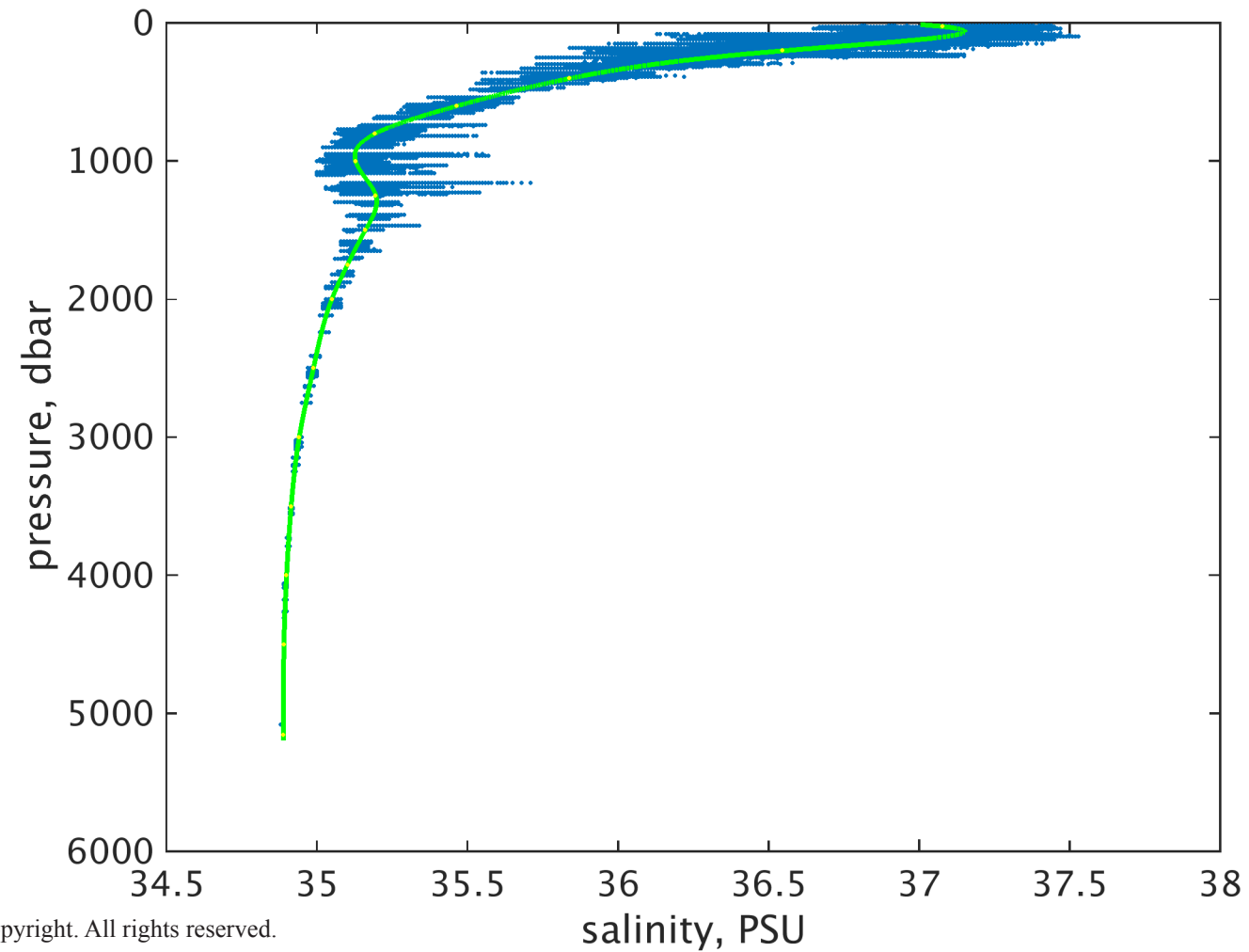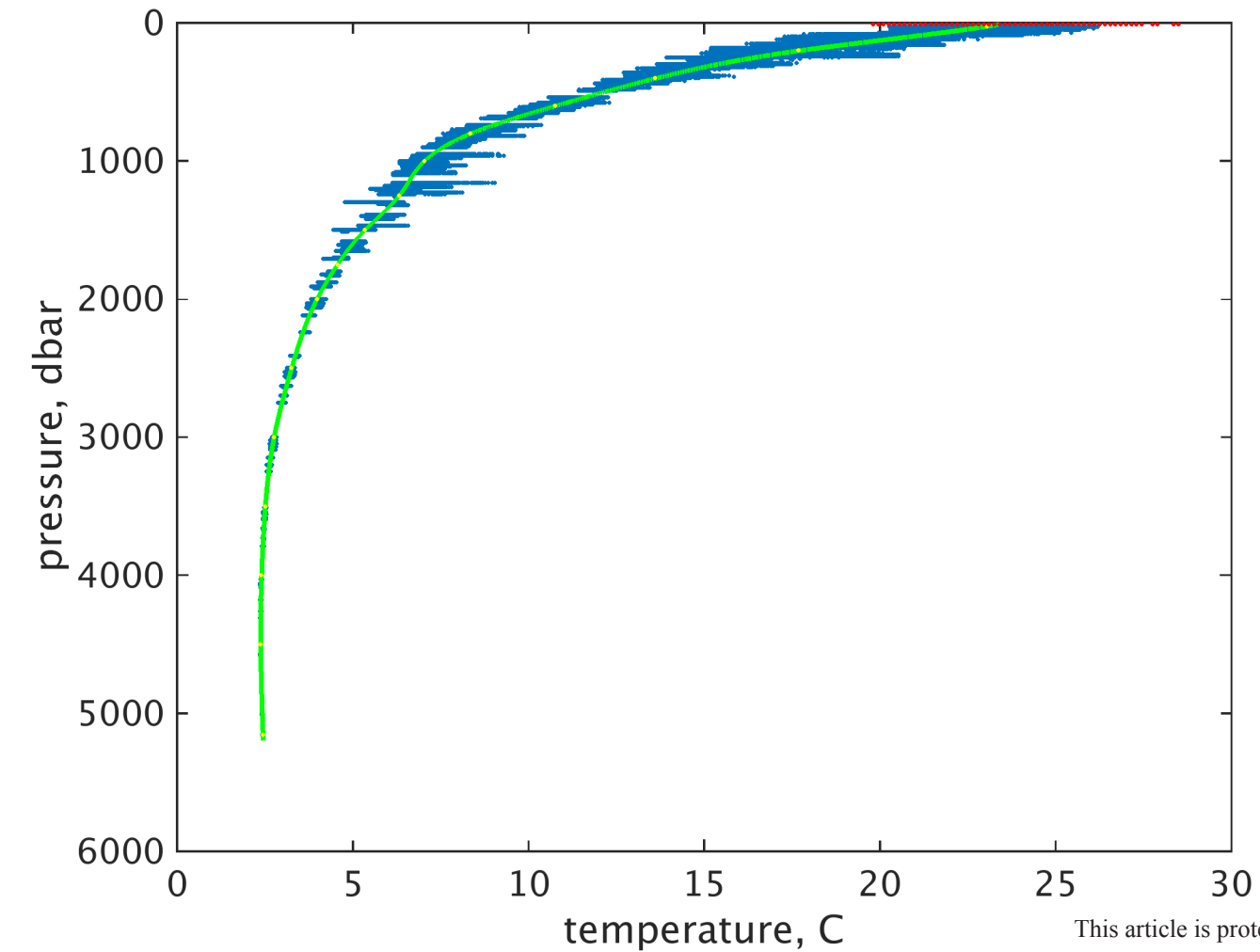
mooring recorded pressure, dbar
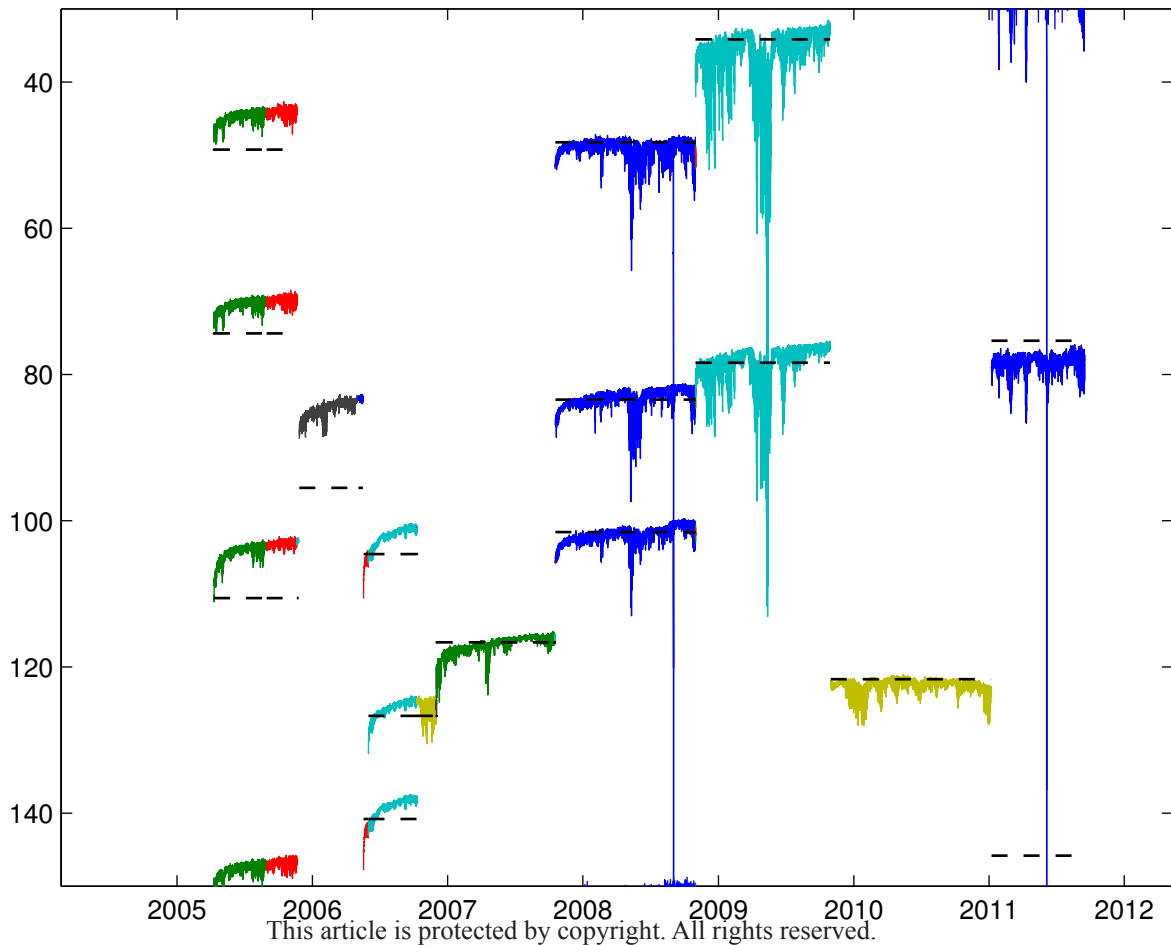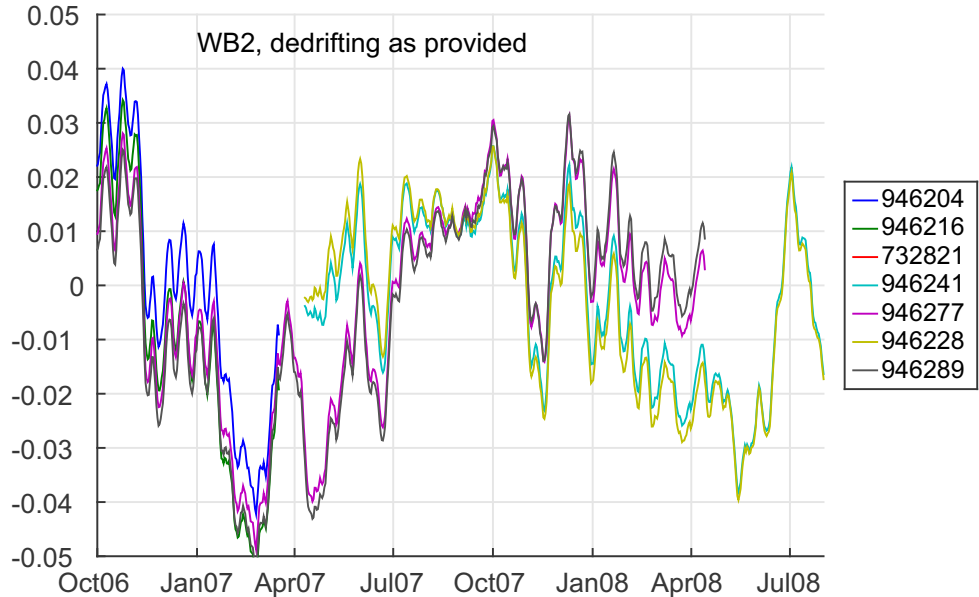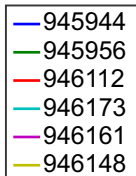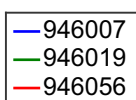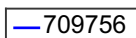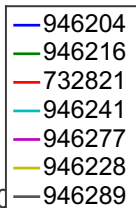
EB1 mooring, monthly mean of sample at altimetry dates

(a) Altimetry, cm — SSH from altimetry

(b) BP anomaly, mbar — No SST

(c) BP anomaly, mbar — Using SST

- P constructed
- instrument error
- vertical sampling error
- P recorded range

(d) Instr. pressure, dbar
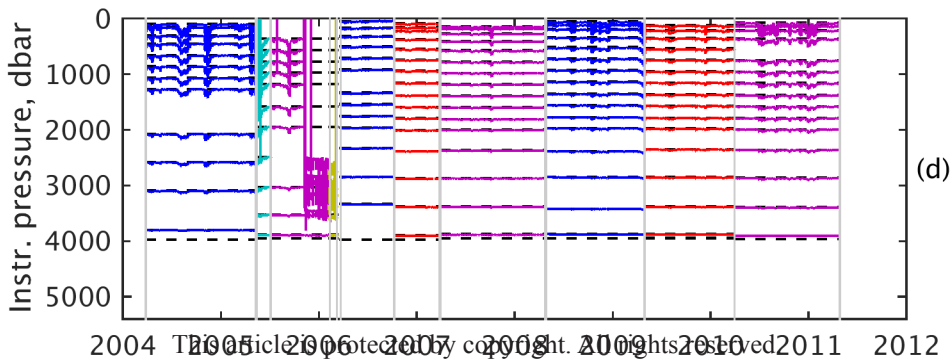
2004 2005 2006 2007 2008 2009 2010 2011 2012

MAR1 mooring, monthly mean of sample at altimetry dates

(a) — Altimetry, cm — SSH from altimetry

(b) — BP anomaly, mbar — No SST

(c) — BP anomaly, mbar — Using SST
- P constructed
- instrument error
- vertical sampling error
- P recorded range

(d) — Instr. pressure, dbar
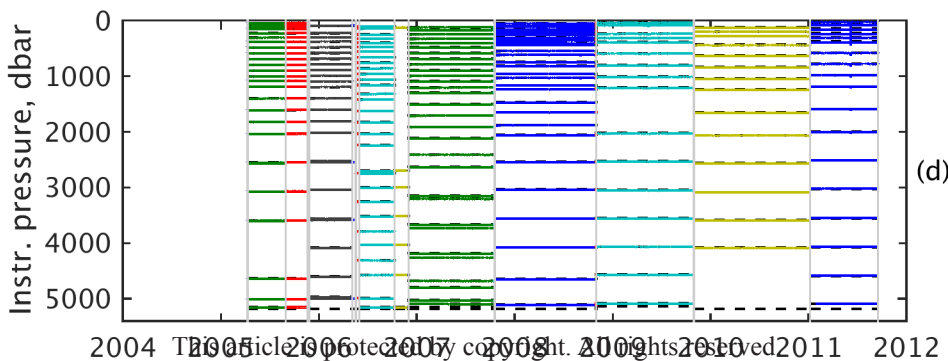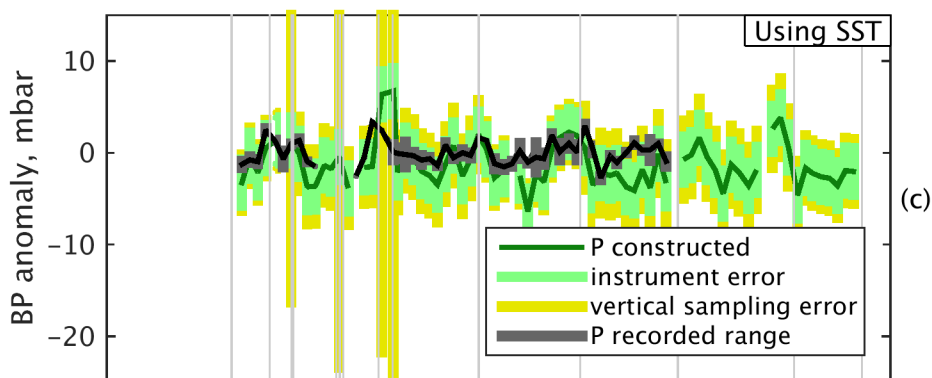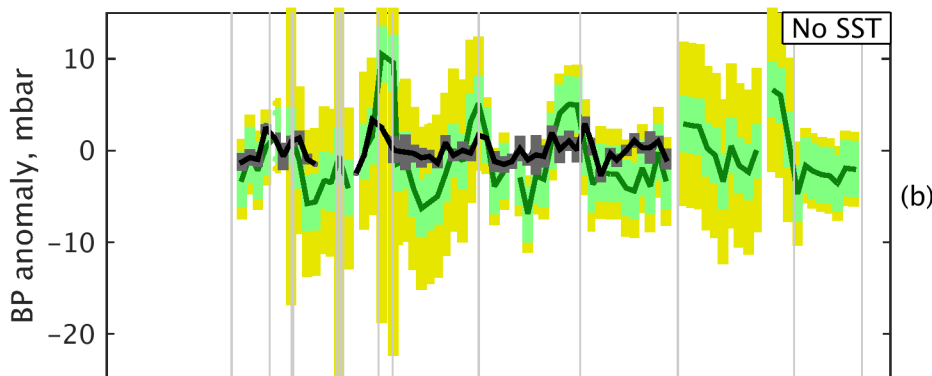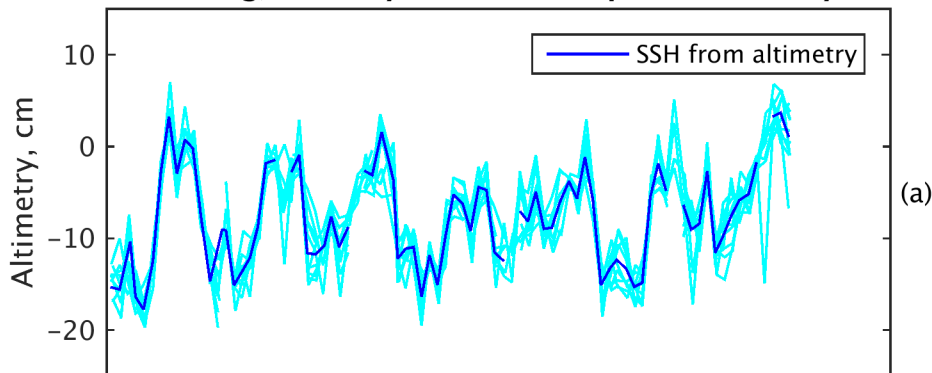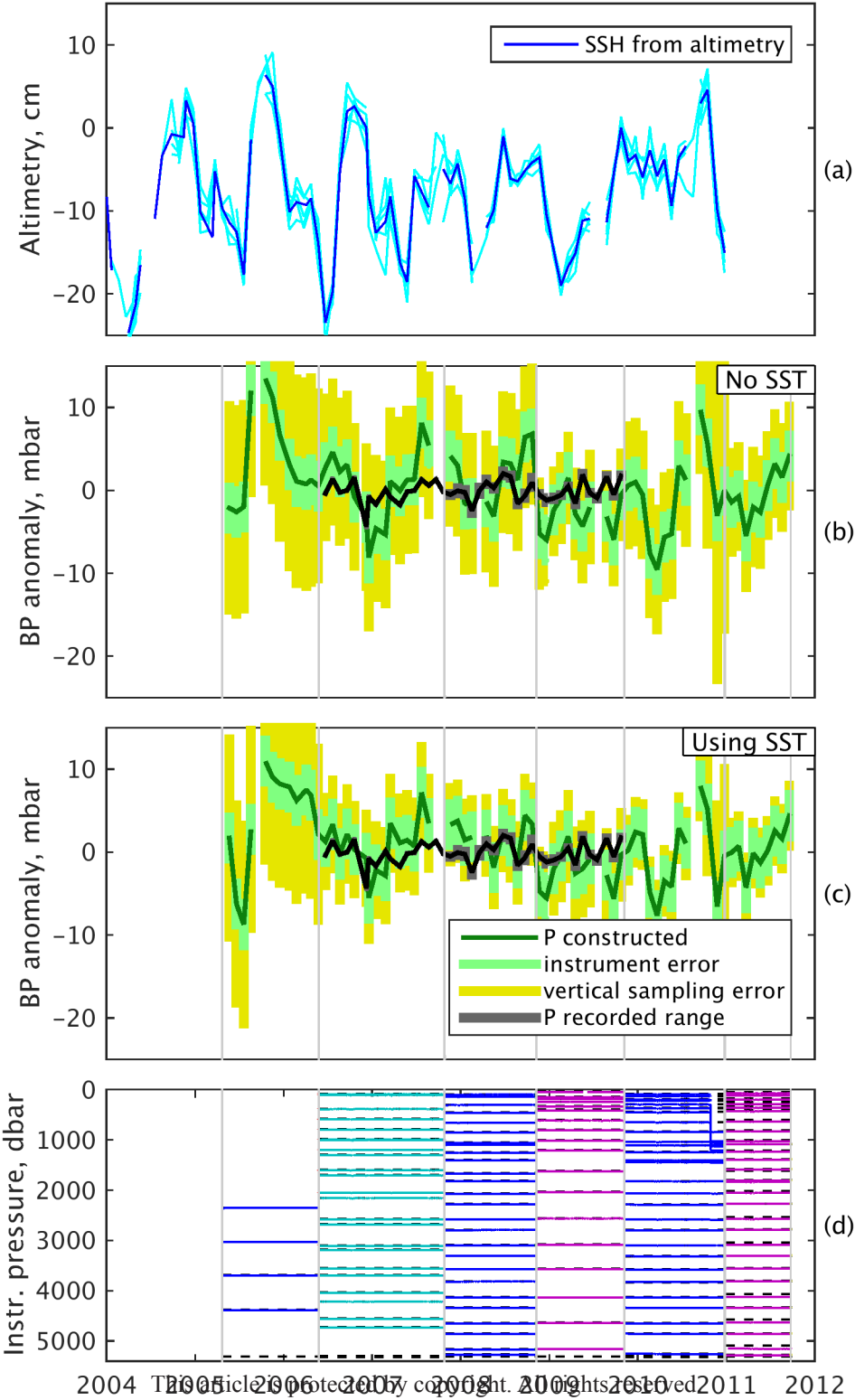
WB5 mooring, monthly mean of sample at altimetry dates

(a)

(b)

(c)

(d)

WB2 mooring, monthly mean of sample at altimetry dates

(a) Altimetry, cm — SSH from altimetry

(b) BP anomaly, mbar — No SST

(c) BP anomaly, mbar — Using SST
- P constructed
- instrument error
- vertical sampling error
- P recorded range

(d) Instr. pressure, dbar

2004 2005 2006 2007 2008 2009 2010 2011 2012
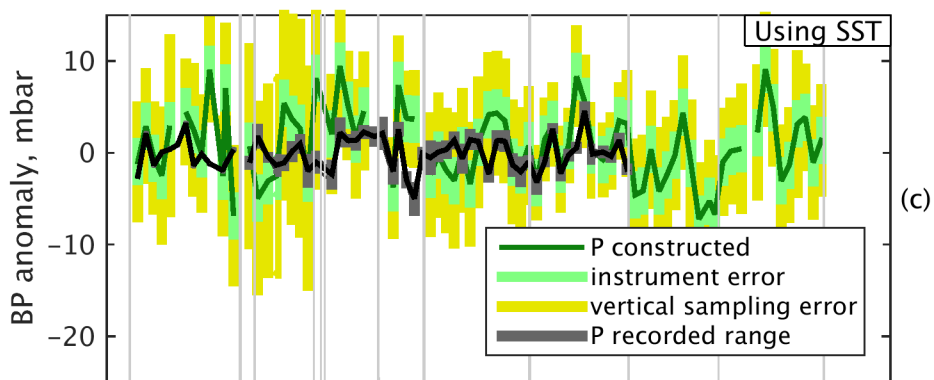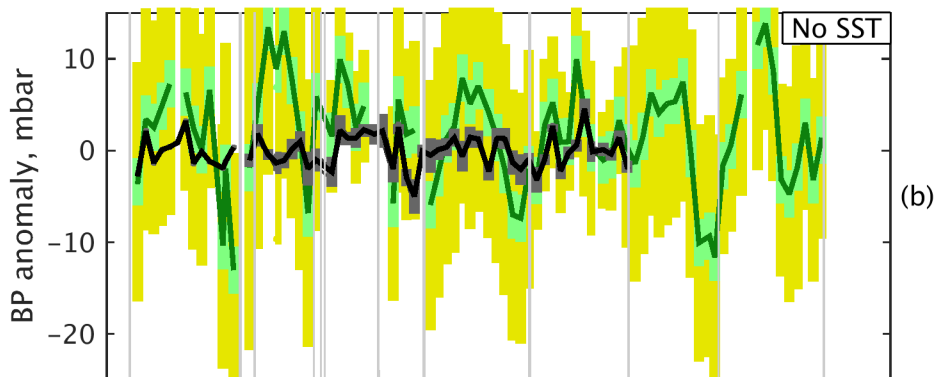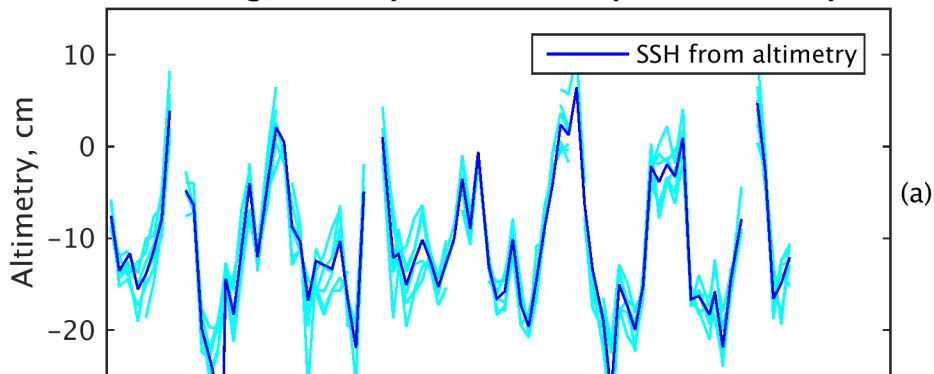
Trend detection, subsampled bp from NEMO with noise, at EB1
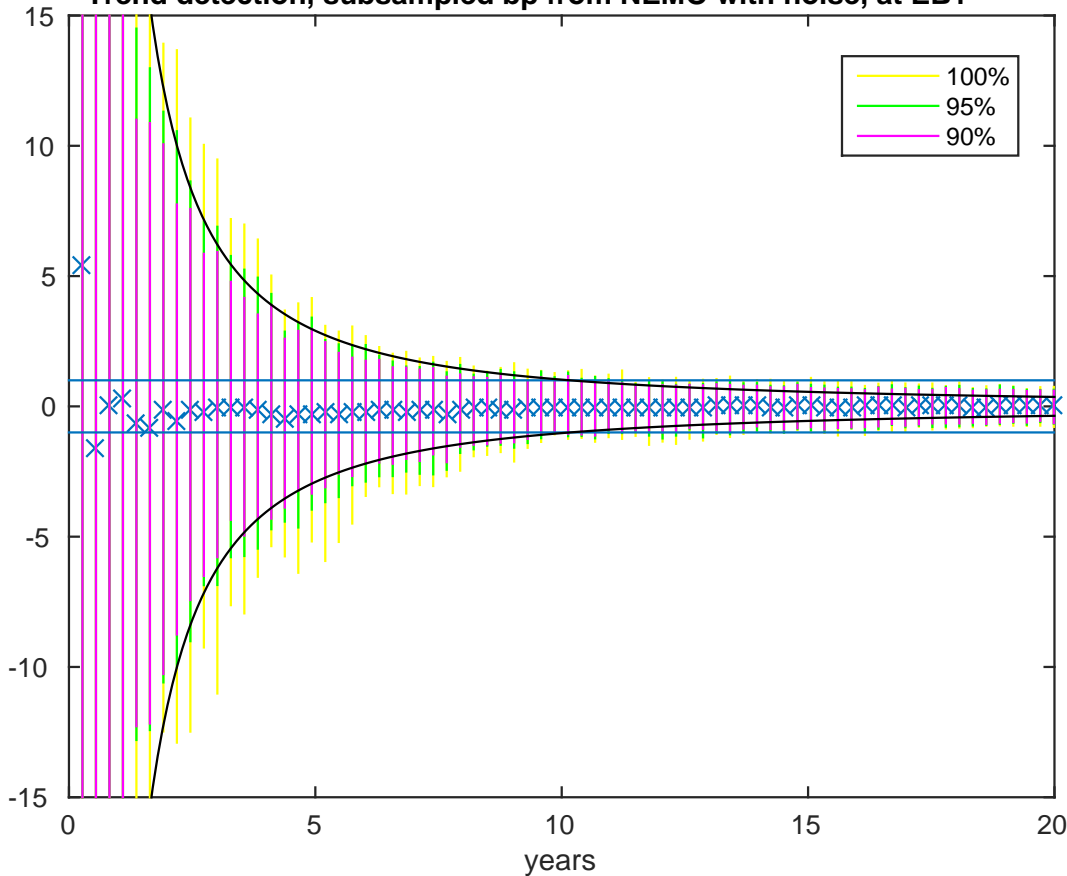
Trend detectable in given time, steric+alt constructed bp at EB1